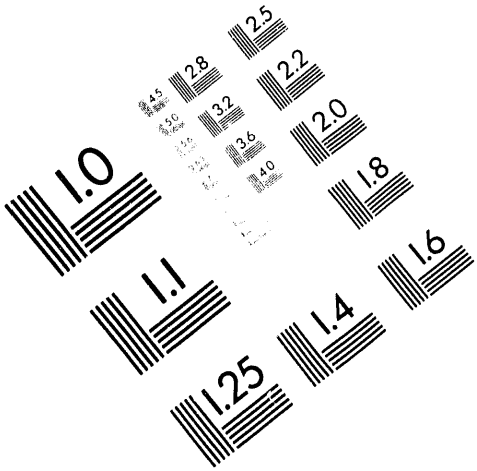

Association for Information and Image Management

1100 Wayne Avenue, Suite 1100
Silver Spring, Maryland 20910

301/587-8202

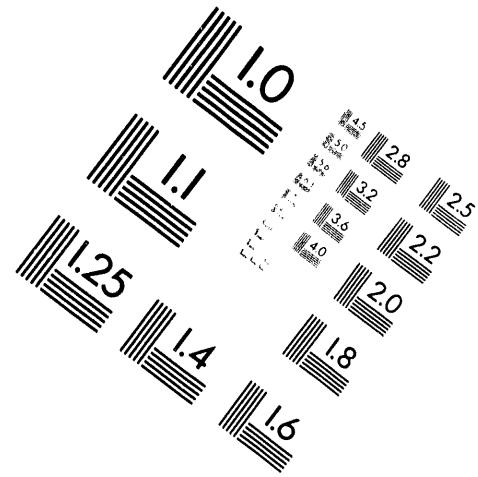

Centimeter

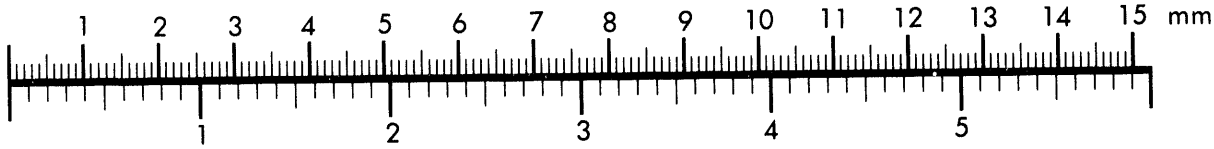

Inches

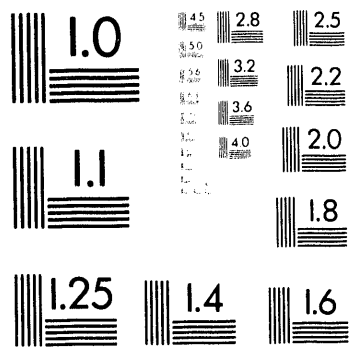

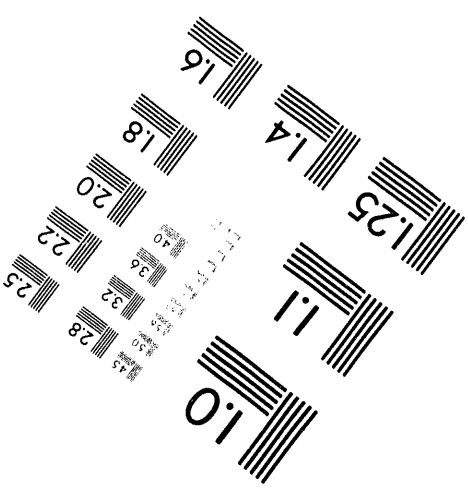

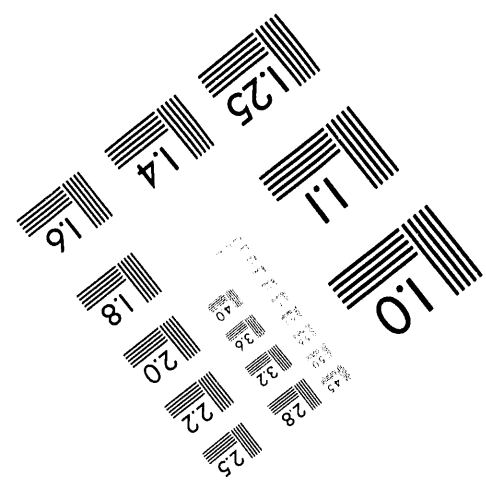

MANUFACTURED TO AIIM STANDARDS
BY APPLIED IMAGE, INC.

1 of 1

LA-12811-MS

UC-504 and UC-520
Issued: August 1994

Mechanical Behavior of $^{238}UO_2$, $^{238}PuO_2$, and $^{239}PuO_2$ as a Function of Strain Rate and Temperature

M. G. Stout
R. W. Ellis
R. A. Pereyra

DISTRIBUTION OF THIS DOCUMENT IS UNLIMITED

Los Alamos
NATIONAL LABORATORY
Los Alamos, New Mexico 87545

MASTER

Table of Contents

ABSTRACT 1

1. Introduction 1

2. Experimental Procedures 4
   2.1. Specimen Preparation 4
   2.2. Mechanical Testing 5
   2.3. Stoichiometric Analysis 7

3. Experimental Results 7
   3.1. Compression Experiments 7
   3.2. Stoichiometric Analyses 10
   3.3. Microscopic Studies 11
      3.3.1. Hot-Pressed and Grain-Stabilized Urania 11
      3.3.2. Cold Pressed and Sintered 13

4. Prediction of Yield Strength and Fracture Stress as a Function of Strain Rate and Temperature 14
   4.1. Mechanical Threshold Stress Model 14
   4.2. MTS Analysis of the Radford and Terwilliger Data 17
      4.2.1. Grain Size 17
      4.2.2. Porosity Effects 18
      4.2.3. Stoichiometry 19
      4.2.4. Corrected Data 19
   4.3. MTS Model Coefficients 19
   4.4. Predictions of the MTS Model 21
   4.5. Urania $^{238}UO_2$, Deformation/Fracture/Yield Strength Maps 21

5. Comparison of $^{238}UO_2$ with $^{238}PuO_2$ and $^{239}PuO_2$ 25
   5.1. Behavior of Plutonia and Urania 25
   5.2. Fracture Map of Plutonia 26

6. Conclusions 28

References 29

MECHANICAL BEHAVIOR OF $^{238}UO_2$, $^{238}PuO_2$, AND $^{239}PuO_2$ AS A FUNCTION OF STRAIN RATE AND TEMPERATURE

by

M. G. Stout, R. W. Ellis, and R. A. Pereyra

ABSTRACT

The mechanical response of $^{238}UO_2$ was measured as a function of strain rate and temperature. We evaluated material produced by two processing schedules: hot pressing followed by a grain stabilization; and cold pressing plus a sintering treatment. The response of these two materials was identical, within the scatter of our data. We complemented our data with that published in the literature, after having made the appropriate corrections for grain size, porosity, and stoichiometry. The entire collection of data was used to evaluate the Follansbee-Kocks mechanical threshold stress (MTS) model for the prediction of yield stress as a function of strain rate and temperature. We used this model to predict the yield stress of $^{238}UO_2$ for strain rates between $\dot{\varepsilon} = 10^{-5}$ and 10^{3} s^{-1} and temperatures from 800° to 1600°C. These predictions provided the basis for constructing a deformation/fracture map for both urania and plutonia. Examination of the maps indicates that for compressive loading and impact strain rates, the $^{238}UO_2$ will be an excellent mock material for $^{238}PuO_2$. Under these conditions both the strength and deformation and the fracture modes are consistent between these two materials.

1. Introduction

For deep-space probes such as Galileo and Ulysses, radioisotope thermoelectric generators (RTGs) are used as the power source. The 'fuel' for these electric power generation systems is $^{238}PuO_2$. An extensive safety analysis is necessary to use nuclear materials in space applications. Potential accident scenarios to be considered are launch-pad explosions, failure to achieve orbit, and earth reentry during flyby. An extensive series of engineering systems experiments including module impact tests, fragment impact tests, and rocket-sled experiments have been, and will continue to be, conducted to verify the resistance of the RTGs to these potential accidents. It is not always possible to use $^{238}PuO_2$ in these studies because of the potential for serious radioactive contamination. We have used $^{238}UO_2$ as a mock material for the plutonia in many of the safety studies because $^{238}UO_2$ is radiologically very benign, being only a mild beta particle emitter. An analysis of the possible accident conditions provides a range of temperatures and strain rates that might be experienced and include strain rates between 10^{-4} s^{-1} and 10^{4} s^{-1} and temperatures between 900° and 1400°C. This study was undertaken to verify that $^{238}UO_2$ is in fact an appropriate mock material for plutonia over these strain rates and temperature regimes and to understand the mechanisms by which urania deforms and fractures.

In this study we were principally concerned with the mechanical response, deformation, and fracture of urania. We conducted this investigation to determine conditions where urania

undergoes plastic deformation and postulated the mechanism by which the deformation is accomplished. These results permitted us to evaluate a relationship to predict the yield strength of $^{238}UO_2$ as a function of temperature and strain rate. We also conducted a metallographic analysis to determine the fracture mode of urania and to note the conditions under which urania must fracture and cannot deform plastically. Our experiments and the collection of data published in the literature have allowed us to construct maps that predict the performance of urania in the strain rate/temperature regime of accident scenarios. Finally, we have compared our results and predictions of the behavior of urania to data taken previously for $^{238}PuO_2$ and $^{239}PuO_2$. From this analysis we have been able to draw several conclusions concerning how good $^{238}UO_2$ is for simulating plutonia and under what conditions it can be used as a valid simulant.

Both urania and plutonia have the fluorite crystal structure (CaF_2).[1,2] This structure can be thought of as a face centered cubic (f.c.c.) structure of metal ions, with oxygen ions contained in the tetrahedral holes (Figure 1). Both urania and plutonia differ from other metal oxides in that the metal ions are substantially larger than the oxygen ion. The Burger's vector of the fluorite structure, by inspection, is $1/2\langle 0\bar{1}1\rangle$, as it is the shortest lattice vector. However, the choice of slip plane is not nearly as clear. Researchers have reported $\{100\}$ as the primary slip plane[3-5] but have also observed evidence of dislocation activity on the $\{110\}\langle 0\bar{1}1\rangle$[3,4] and $\{111\}\langle 0\bar{1}1\rangle$[5] slip systems as well. Slip systems in addition to the $\{100\}\langle 0\bar{1}1\rangle$ are needed to satisfy compatibility. These investigators have conducted mechanical deformation experiments on single-crystal urania as well as electron microscopy and slip line analyses. Single crystals of urania exhibit extensive plastic deformation, up to 10% strain, at temperatures as low as 600°C.[4] At and above 1000°C the crystals yielded and then deformed at a nearly constant stress. In other words, the behavior was nearly elastic/perfectly plastic. Thus, there is ample evidence that thermally activated dislocation mechanisms control the yield and work hardening of urania single crystals between 900° and 1400°C, the temperature range in which we are interested.

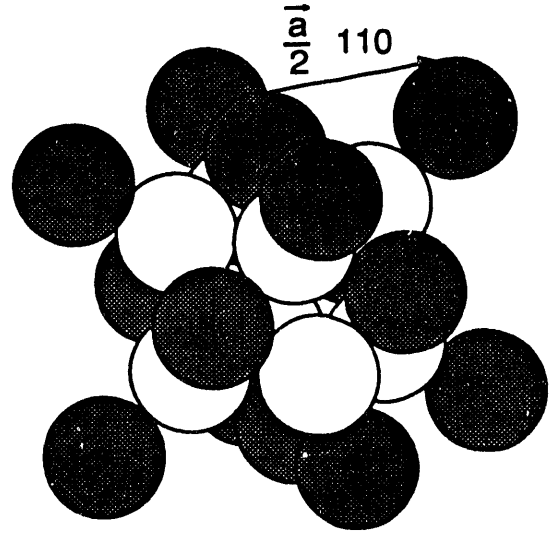

Figure 1 Schematic of the unit cell of stoichiometric UO_2, from Heuer, Keller and Mitchell.[2]

Mechanical property investigations to measure the yield behavior of polycrystalline $^{238}UO_2$ have used compression specimens and various gas mixtures to control stoichiometry. The most extensive collection of data has been reported by Radford and Terwilliger,[6] who examined strain rates between $1.33 \times 10^{-5}\ s^{-1}$ and $2.71 \times 10^{-3}\ s^{-1}$ and temperatures from 600° to 1600°C. In addition, these investigators also examined the effects of grain size. Their data for grain sizes

between 6.3 μm and 17 μm correlate directly to the materials produced at Los Alamos that we used in our study. Nadeau[3] and Byron[7] have also performed compression experiments on urania but over a more limited regime of temperature and strain rate. All of these data show a smooth continuous decrease in yield strength with increasing temperature up to at least 1600°C (with the exception of data from Radford and Terwilliger for a 1 μm grain size material). The strength decrease is not linear but rather approximates an exponential form $\sigma = Ce^{a/T}$, where C and a are constants. The constant C is the strength that the material asymptotically approaches with increasing temperature. These literature data have a yield strength of ~ 300 MPa at 800°C and a nominal strain rate of 10^{-3} s^{-1}. The strength decreases to ~ 40 MPa at 1600°C.

One can use the relationship $(\sigma_1/\sigma_0) = (\dot{\varepsilon}_1/\dot{\varepsilon}_0)^{1/m}$, where σ_0 and $\dot{\varepsilon}_0$ are a reference yield stress and strain rate, to approximately model the strain-rate dependency of the yield stress. Using this relationship Radford and Terwilliger[6] and Nadeau[3] found values for m between 10 and 32. These values for m are typical of a body centered cubic (b.c.c.) metal and indicate that yield occurs as a result of thermally activated dislocation activity. If yield resulted from a grain boundary sliding mechanism, one would expect to measure a value of $m \sim 3$. This is not the case for these experiments, although such numbers have been measured at much lower strain rates, typically $\dot{\varepsilon} \leq 10^{-6} s^{-1}$.

Radford and Terwilliger[6] also studied the effects of grain size; they tested material at a constant strain rate over a variety of temperatures at grain sizes of 17, 9.9, 6.3, and 1.0 μm. We interpreted their data slightly differently than they did and used a narrower range of grain sizes. If we examine their data only for the materials with the 17, 9.9, and 6.3 μm grain sizes, between 800° and 1400°C, we find that the yield stress is related to the grain size by a relationship that has the form of the classic Hall-Petch relationship: $\sigma_0 = b + K/\sqrt{d}$, where b and K are arbitrary constants and d is the grain size of the material. The temperature dependency of yield strength is accounted for in the term b while K is constant with respect to temperature, K = 391 MPa$\sqrt{\mu m}$. The values of b did not remain positive as needed to make physical sense, if the relationship were valid for *all grain sizes* of material. However, we believe that the relationship can be used to account for grain size effects specifically between 17 and 6 μm, or close to these grain sizes, and over the temperature range of our experiments from 900° to 1400°C.

Previous results have shown that oxygen stoichiometry very strongly affects the yield strength of $^{238}UO_2$.[3,5,7] Using a controlled CO/CO_2 gas mixture to specify the exact stoichiometry of polycrystalline material, Nadeau[3] found that the yield strength decreased extremely rapidly for even small amounts of oxygen in excess of 2.0. For example, polycrystalline material with a composition of $^{238}UO_{2.01}$ had a 30% lower yield strength than stoichiometric $^{238}UO_2$. Byron[7] tested stoichiometric urania in a dry helium atmosphere with graphite rams to provide compressive loading. We found that a similar situation using graphite heating elements and a dry helium atmosphere acts to reduce the urania. Byron's[7] results also showed a decrease in yield strength for temperatures between 600° and 1600°C, from that which he measured using a purified argon atmosphere and an absence of graphite (this condition would have left

stoichiometric $^{238}UO_2$). Thus, it appears that if the urania is either slightly hypo- or hyper-stoichiometric, a decrease in the yield and flow strength results.

Bend experiments have been used to study the fracture behavior of $^{238}UO_2$ as a function of temperature and strain rate.[8-11] Using the standard strength and materials equations for a beam, the outer ligament tensile stresses were calculated at the point that the bend bars either failed or began to exhibit extensive plastic deformation. Both Evans and Davidge[8] and Canon *et al.*[9] divided the fracture behavior into different regions depending on the extent of observed plastic deformation. They found that below ~ 1050°C the bend bars fractured in a purely brittle manner, irrespective of grain size or bending strain rate. Between 1050° and 1400°C they began to observe some plasticity, from bending in the bars, and above 1400°C ($\dot{\varepsilon} = 2.56 \times 10^{-5}\ s^{-1}$) there was moderate deformation and a rapid decrease in the yield stress of the bars associated with grain boundary sliding.[9] At higher strain rates the temperature at which this transition of deformation mechanism occurred increased. Canon *et al.* found that the fracture stress of the bend bars was nearly constant up to the temperature where grain boundary sliding became a dominant deformation mechanism. The stress they measured was about 145 MPa and nearly grain-size and strain-rate independent, $2.56 \times 10^{-4}\ s^{-1} < \dot{\varepsilon} < 2.56 \times 10^{-3}\ s^{-1}$. Evans and Davidge reported similar results. However, they also observed a slight peak in the fracture stress at the temperature where plastic deformation was first observed, ~ 1050°C. These results (Refs. 8 and 9) were for material that was 97% to 98% of theoretical density. Roberts and Ueda[10] looked at the effects of porosity. Bend bars were prepared using naphthalene to create porosity. During sintering the naphthalene was eliminated leaving a porous structure. Various porosities were investigated from 4% to 18%. The strengths, at 1250°C, ~ 100 MPa, measured for bars that were 96% dense, were substantially less than those determined from their other tests on 97% to 98% dense material, prepared without the naphthalen. Roberts and Ueda[10] reported that the ultimate strength increased as the porosity decreased. At densities of the material that we have tested, 85% of theoretical or 15% porosity, they report strengths near 140 MPa. This strength is nearly identical to that which they reported in Reference 10 for 97% to 98% dense material. Thus, from the reported data in the literature, the actual effects of porosity are not particularly clear.

2. Experimental Procedures

2.1. Specimen Preparation

Urania powder with a grain size of 3.6 μm was fabricated into right circular cylinders with a 1:1 aspect ratio. Two fabrication schedules were used; a hot press followed by a grain-stabilization treatment and a cold pressing and sintering. The specific treatments were:

> *Hot Pressing and Grain Stabilization*: Hot press in a 32-mm-diameter die at 1650°C and 20.68 MPa for 0.5 hrs. and then grain stabilize at 1700°C for 2 hrs. The grain-stabilization treatment was conducted under a wet hydrogen atmosphere designed to bring the material stoichiometry to $^{238}UO_2$.

Cold Pressed and Sintered: Cold press in a 41-mm die to 68.945 MPa, cold isostatically press to 344.73 MPa, sinter at 1800°C for 2 hrs. under a wet hydrogen atmosphere, again to attain stoichiometric $^{238}UO_2$.

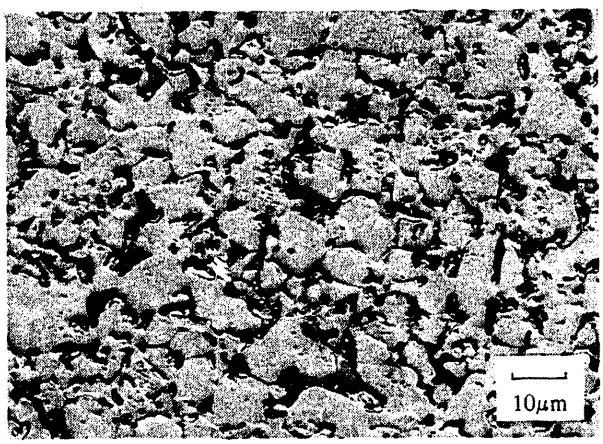

Figure 2 Microstructure resulting from the hot-pressing and grain-stabilization fabrication technique.

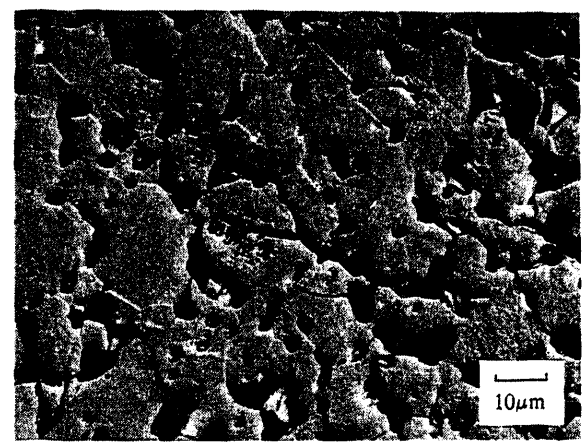

Figure 3 Microstructure resulting from the cold-pressed and sintered technique.

These two treatments produced material that was between 83% and 87% of theoretical density with a grain size (determined by a linear intercept method) of 5.2 μm and 7.1 μm, respectively. The resulting microstructures are shown in Figures 2 and 3 for the hot- and cold-pressed materials. Microstructurally, there does not appear to be any major difference between materials produced by the two different techniques, either in grain size or shape or in the morphology of the porosity. In the case of the cold-pressed and sintered material, the grains have grown slightly and the porosity coalesced.

Cylinders 9.6 mm in diameter were cored ultrasonically from the larger cylinders and then sectioned to give compression specimens 9.6 mm long. Three cores were cut from each large cylinder, and then each of these cores yielded two specimens. The final preparation technique was to grind the ends of the specimens to guarantee they were parallel and perpendicular to the cylindrical axis.

2.2. Mechanical Testing

Specimens were tested in compression using the furnace and load train shown in Figure 4. The furnace is contained in a stainless steel environmental chamber that is double-walled and water-cooled. Water-cooled stainless steel loading pistons penetrate the environmental chamber, through O-ring seals, to load the specimen. Alignment of these loading rams is provided by translational ball bearings mounted to the environmental chamber. A single 'through rod' is used

to provide initial alignment of the bearings. Heating in the chamber is by means of two graphite heating elements, surrounding the specimen. The heaters are large enough that the specimen, platens, and tips of the loading rams are in the hot zone. A series of graphite shells enclose the heaters and function as heat shields to minimize radiant heat losses. There is a tungsten/zirconium/molybdenum (TZM) spherical seat on the tip of the top compression ram to provide for final alignment. Load is transferred to the specimen from the compression rams; first to a graphite platen, then an alumina platen, and finally a thin sheet of Grafoil graphite to act as a lubricant. This stacking sequence is the same on both the top and bottom of the sample. We measured the temperatures with a platinum-10% rhodium thermocouple that was placed in immediate proximity to the specimen. Finally, the entire furnace assembly is mounted to an Instron Type TT-B-L mechanical testing system (c. 1950). With this test system we conducted experiments at the highest and lowest possible crosshead displacement rates: 50.8 and 1.27 mm/min. These displacement rates corresponded to strain rates of 0.1 s^{-1} and 2.5 x 10^{-4} s^{-1} for our particular specimen geometry.

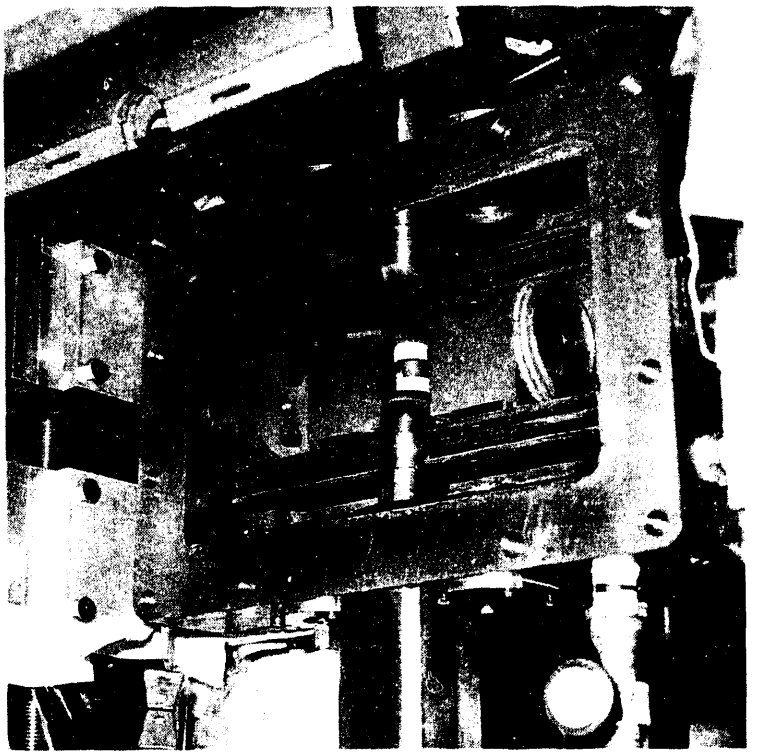

Figure 4 Photograph of the experimental compression testing equipment showing the environmental chamber, furnace elements, radiant heat shields, and load train.

We used the conventional Instron load cell for measurement of load. The load-cell excitation and signal conditioning was by means of a Vishay model 2310 signal-conditioning amplifier, and the data was recorded with a Data Precision model 611 digital oscilloscope. Because of the furnace, environmental chamber, and load train, it was impossible to measure actual specimen displacements. However, we did measure crosshead displacements during testing with a linear voltage differential transducer (LVDT).

In an experimental setup such as this one, the load train is relatively 'soft'; in other words, a large part of the displacement measured by the LVDT results from deflection of the load train and not deformation of the specimen. We ran a compliance calibration on the load train at each of our test temperatures without a specimen in place, to measure this compliance. This calibration was then used to remove any load train displacements from our experimental data; hence, we could 'back out' the actual specimen displacements from our experimental LVDT measurement.

2.3. Stoichiometric Analysis

We analyzed the stoichiometries of the starting hot- and cold-pressed materials and specimens after testing. The specimens selected for oxygen analysis were ones tested at 1400°C at both strain rates. Preliminary results suggested that the materials might begin in a slightly hyperstoichiometric condition and then be reduced, from the carbon furnace elements during the course of testing, to a hypostoichiometric condition. For measuring stoichiometry the material of interest was placed in a quartz boat, weighed, and then oxidized by heating at 1000°C in air to $^{238}U_3O_8$. Subsequently, the specimen was reduced at 1000°C in a 6% hydrogen argon gas mixture to $^{238}UO_2$ and reweighed. By comparing the initial and final weights, the exact stoichiometry, x, was determined to within ±0.003 for $^{238}UO_x$.

3. Experimental Results

3.1. Compression Experiments

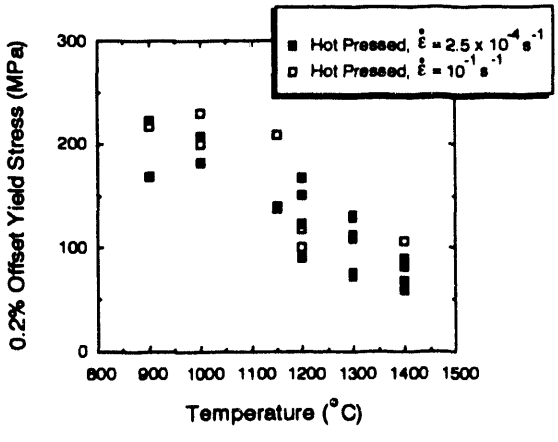

Figure 5 Experimentally measured yield strengths as a function of temperature, for strain rates of ε = 0.1 s^{-1} and 2.5 x 10^{-4} s^{-1}, for the hot-pressed and grain-stabilized urania.

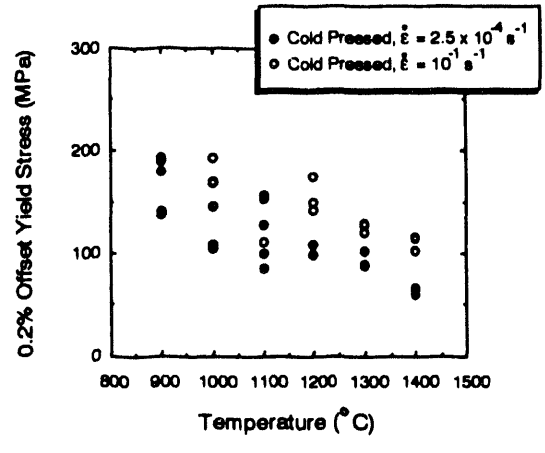

Figure 6 Experimentally measured yield strengths as a function of temperature, for strain rates of ε = 0.1 s^{-1} and 2.5 x 10^{-4} s^{-1}, for the cold-pressed and sintered urania.

Our experimental results are summarized in Figures 5 and 6. We plotted the 0.2% offset yield strengths of the hot- and cold-pressed materials, respectively, as a function of temperature for the two strain rates $\dot{\varepsilon}$ = 0.1 s^{-1} and 2.5 x 10^{-4} s^{-1}. Both materials have a yield strength of about 200 MPa at 900°C. The measured yield strengths then decrease continuously to a minimum of 70 MPa at 1400°C. We observed that both materials were slightly strain-rate sensitive; the open circles and squares, $\dot{\varepsilon}$ = 0.1 s^{-1}, lie above the closed circles and squares, $\dot{\varepsilon}$ = 2.5 x 10^{-4} s^{-1}. If we use the approximate equation: $(\sigma_1/\sigma_0) = (\dot{\varepsilon}_1/\dot{\varepsilon}_0)^{1/m}$, where σ_0 and $\dot{\varepsilon}_0$ are a reference yield stress and strain rate, we find $m \approx 25$. This is comparable to the value reported by Nadeau[3] and

Radford and Terwilliger[6] and indicates that yield must occur as a result of dislocation activity rather than a grain boundary sliding mechanism. We combined the data for both materials in Figure 7. There are apparently no differences in the yield behavior between these two materials. The data match one another within our experimental scatter. This is what one might expect for a material where yield is a result of dislocation activity; in this case the yield strengths are controlled by impurities and grain size. Although the $^{238}UO_2$ powders were processed by different thermomechanical schedules, the impurity content of the final compression specimens should have been the same. In addition, the microstructures shown in Figures 2 and 3 indicate that there was very little grain size difference resulting from the two processing schedules.

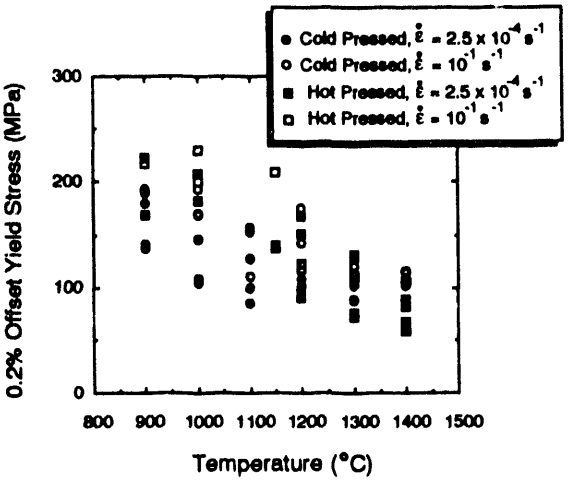

Figure 7 A combination of the yield strength data for both the hot- and cold-pressed urania, ε = 0.1 s^{-1} and 2.5 x 10^{-4} s^{-1}.

The stress/strain responses of these data are shown in Figures 8a-d, and 9a-d. Figures 8 and 9 are for the hot-pressed and grain-stabilized and cold-pressed materials, respectively. We have broken the plots into two temperature ranges, 900° to 1150°C and 1200° to 1400°C, and have plotted each of the strain rates separately. At the beginning of each of these plots, where we know the material is elastic, there is a marked deviation from linearity. This is a result of an initial inaccuracy of our compliance determination and it should be ignored. The behavior of the material appears to be a very strong function of the yield stress. Roughly speaking, the response can be split into two categories, yield below 140 MPa and yield above 160 MPa. If the material yield strength is above 160 MPa, we observe elastic behavior, and then in almost all cases, a catastrophic failure. This failure is often followed by an immediate load drop, particularly at the higher strain rates. When the material yields below 140 MPa, we typically observe an extended region of plastic deformation that can exceed 10% strain. The deformation is characterized by continuous hardening at a very low rate. Thus, one can think of the behavior as nearly elastic/perfectly plastic. Occasionally, specimens experienced early fracture, even when the yield strength was below 140 MPa. This is likely attributable to either a preexisting large flaw in the material or a deviation from stoichiometry. Behavior of a similar nature was observed by Byron[7] for material that had a stoichiometry of $^{238}UO_{2.02}$.

Specimens tested at 1150° and 1100°C yield near 150 MPa and could be characterized by behavior that appears to be transitioning between ductile plasticity and brittle fracture. Immediately after yield the material flows plastically but then begins to crack. The cracking appears as a drop in the load displacement curve. In several cases after the load drop, the specimen was able to reload to its previous level and continue hardening for a short period of time. The stress/strain behavior that we observed correlates with temperature. The yield stresses

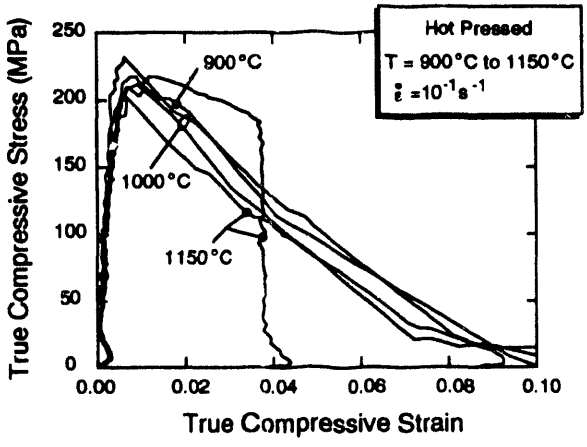

Figure 8a Stress/strain behavior of the hot-pressed and grain-stabilized urania at temperatures of 900, 1000, and 1150°C and a strain rate of ε = 0.1 s^{-1}.

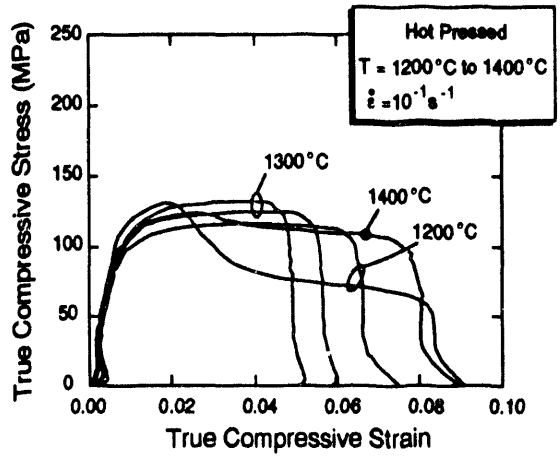

Figure 8b Stress/strain behavior of the hot-pressed and grain-stabilized urania at temperatures of 1200, 1300, and 1400°C and a strain rate of ε = 0.1 s^{-1}.

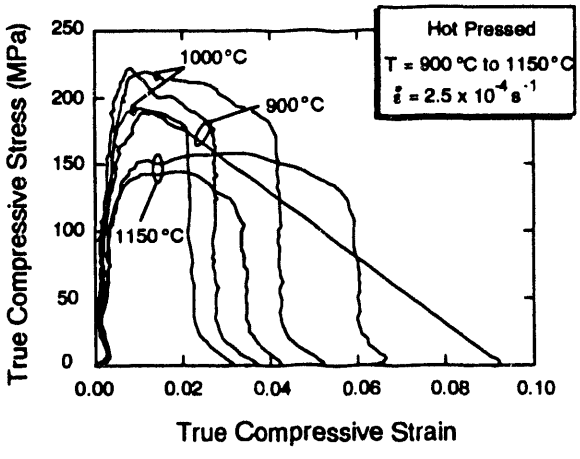

Figure 8c Stress/strain behavior of the hot-pressed and grain-stabilized urania at temperatures of 900, 1000, and 1150°C and a strain rate of ε = 2.5 x 10^{-4} s^{-1}.

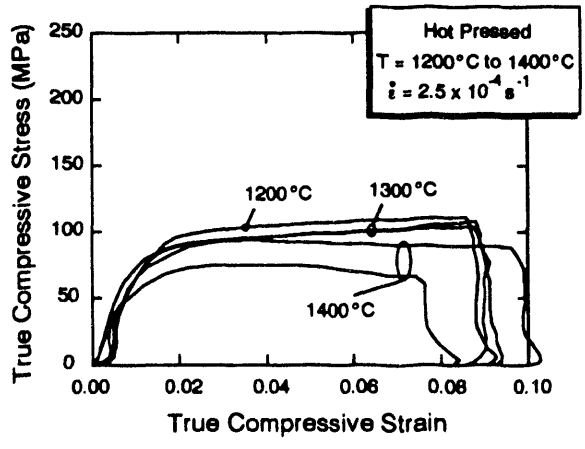

Figure 8d Stress/strain behavior of the hot-pressed and grain-stabilized urania at temperatures of 1200, 1300, and 1400°C and a strain-rate of ε = 2.5 x 10^{-4} s^{-1}.

at or below 140 MPa were associated with experiments conducted at or above 1200°C. At temperatures below 1100°C, dislocation activity is much more restricted. This results in the higher yield stresses. The diameter of the material must expand as it is compressed. To accomplish this, plastic flow and dislocation activity are necessary to maintain compatibility between the grains of material. Because of the limited dislocation activity below 1100°C, as evidenced by the high yield stresses, it was impossible for the material to maintain this

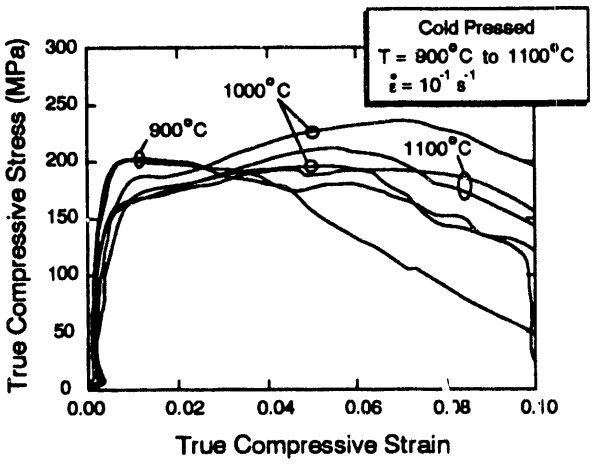

Figure 9a Stress/strain behavior of the cold-pressed and sintered urania at temperatures of 900, 1000, and 1100°C and a strain rate of $\varepsilon = 0.1\ s^{-1}$.

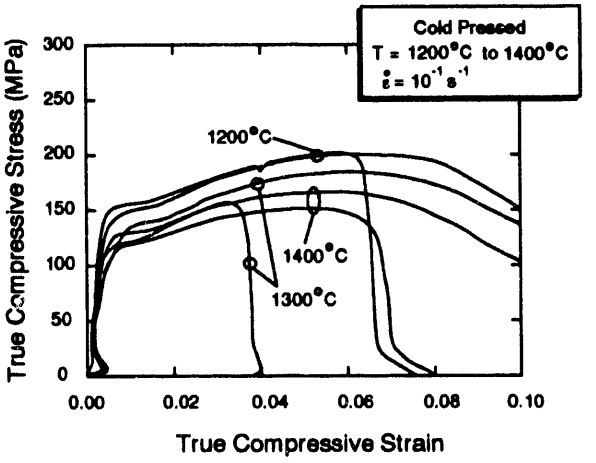

Figure 9b Stress/strain behavior of the cold-pressed and sintered urania at temperatures of 1200, 1300, and 1400°C and a strain rate of $\varepsilon = 0.1\ s^{-1}$.

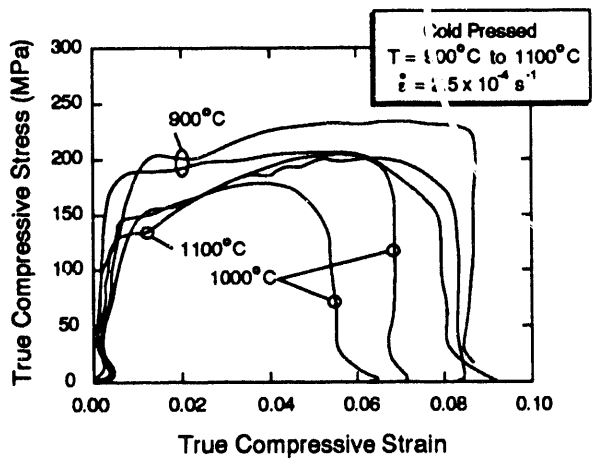

Figure 9c Stress/strain behavior of the cold-pressed and sintered urania at temperatures of 900, 1000, and 1100°C and a strain rate of $\varepsilon = 2.5 \times 10^{-4}\ s^{-1}$.

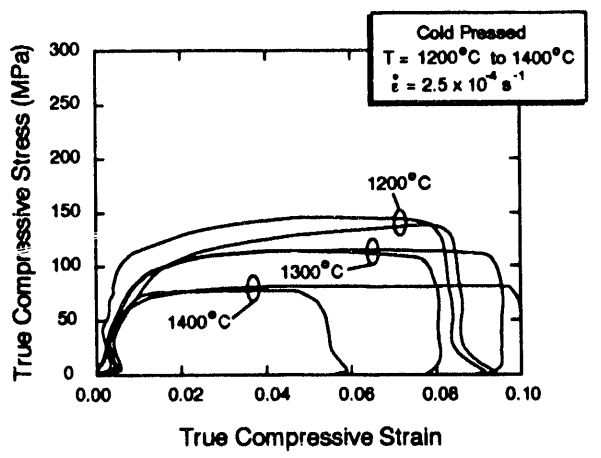

Figure 9d Stress/strain behavior of the cold-pressed and sintered urania at temperatures of 1200, 1300, and 1400°C and a strain rate of $\varepsilon = 2.5 \times 10^{-4}\ s^{-1}$.

compatibility. The result is very localized heterogeneous tensile stresses, normal to the axis of compression. We believe that these stresses resulted in the catastrophic failures that we observed.

3.2. Stoichiometric Analyses

The results of our stoichiometric analyses are presented in Table I. We measured the

stoichiometry in both virgin and tested materials. Both the virgin cold-pressed and sintered and hot-pressed materials were extremely close to stoichiometric $^{238}UO_2$; in addition, the stoichiometry of material from the outer periphery of the fabricated pellets matched that of material cut from the pellet's core. Our examination of the tested specimens showed that the testing conditions, vacuum and exposure to graphite, did very little to alter the materials' stoichiometry. The tested materials were slightly hypostoichiometric, but only by 0.25%. The only exception was a specimen tested at 1400°C and the lower strain rate of $\dot{\varepsilon} = 2.5 \times 10^{-4}\ s^{-1}$, the worst possible case. In this case the material was ~ 0.5% hypostoichiometric.

Table I
Results of the Oxygen Stoichiometric Analysis

Condition	Test Temperature (°C)	Test $\dot{\varepsilon}$ (s^{-1})	x, ($^{238}UO_x$) ± 0.003
hot pressed and grain stabilized	900	2.5×10^{-4}	1.997
hot pressed and grain stabilized	1300	0.1	2.001
cold pressed and sintered	900	2.5×10^{-4}	1.993
cold pressed and sintered	1400	2.5×10^{-4}	1.989
cold pressed and sintered	-	-	2.010
hot pressed and grain stabilized, outer edge	-	-	1.994
hot pressed and grain stabilized, pellet core	-	-	1.991

3.3. Microscopic Studies

3.3.1. Hot-Pressed and Grain-Stabilized Urania

Figure 10 is a low magnification micrograph taken from the cross section of a specimen deformed at 1400°C, $\dot{\varepsilon} = 2.5 \times 10^{-4}\ s^{-1}$. This specimen was compressed along a vertical axis. One of the most noticeable features is that there is substantial cracking over long distances that is not parallel to the compression axis. Ordinarily, this would not be expected, and it suggests

that flaws, or long cracks, existed in the specimens prior to testing. These specimens were deformed at quasi-static strain rates, and thus we would not expect this phenomenon to be the result of rate effects.

We observed both intergranular and transgranular cracking in this specimen's cross section, shown in Figures 11a and 11b, respectively. Cracks that were transgranular appeared to be of a nonvertical nature. It is possible that those were introduced previous to the compression experiment, perhaps during fabrication. Vertical cracking, cracking in the direction expected from deformation, was typically intergranular at these temperatures. Although both transgranular and intergranular cracking were observed, the greatest fraction of cracking was intergranular at both 1300°C and 1400°C. The fractures that we observed were very localized and did not have a diffuse character. It does not appear as though the 'deformation' we observed was a result of widespread grain boundary fracturing or microcracking. There was no evidence of microfracturing either in the bulk of the material or in the vicinity of the main cracks.

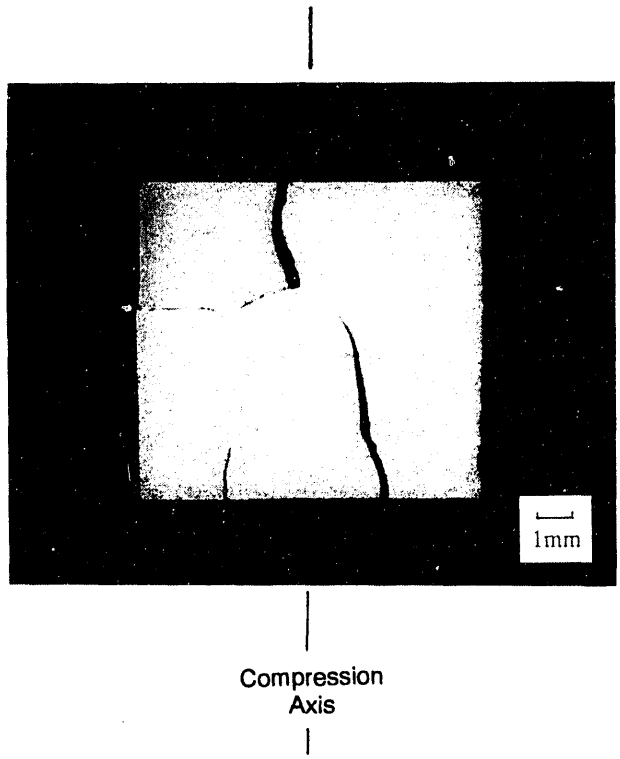

Figure 10 Low magnification micrograph taken from the cross section of a specimen deformed at 1400°C, $\dot{\varepsilon} = 2.5 \times 10^{-4}\ s^{-1}$. Note the macroscopic cracking in a direction normal to the compression axis.

We observed what we believe is recrystallization on the edges of a horizontal transgranular fracture. This region is shown in Figure 12, which is a high magnification micrograph from the cross section shown in Figure 10. The main fracture runs horizontally across the micrograph, perpendicular to the compression axis. A structure of apparently very fine grains lines both the top and bottom surfaces of the crack. The diameter of the fine grains is approximately 1 μm, while the bulk grain size averages 5.2 μm. It is possible that the energy created as a result of plastic deformation, coupled with potential nucleation sites on the internal fractured surface, produced the apparent recrystallization. This hypothesis depends on the crack existing prior to deformation. This feature provides further evidence that the deformation of the urania at 1400°C is a result of thermally activated dislocation motion rather than grain boundary sliding processes.

Figure 13 is a low magnification micrograph of a hot-pressed cylinder tested at 1000°C and a strain rate of $\dot{\varepsilon} = 2.5 \times 10^{-4}\ s^{-1}$. The fractures were much more catastrophic than what we

observed at higher temperatures. Higher magnification micrographs of this specimen illustrate both intergranular (Figure 14a) and transgranular fractures (Figure 14b). Both of these fractures, which are different in nature, are parallel to the compression axis, and we believe that they resulted from the mechanical deformation rather than processing.

In summary, the fracture mode of the hot-pressed material is temperature sensitive. We observed that the fractures resulting from deformation were strictly intergranular at temperatures of 1300°C and 1400°C. This result was insensitive to the particular strain rates that we studied. It is possible, however, that if the strain rates were elevated above 0.1 s^{-1} at 1300° and 1400°C, we would observe transgranular fracture. This is speculation, as we have no experimental evidence from such conditions at this time. At 1000°C the fracture mode was a mixture of transgranular and intergranular. Both of these fracture modes were the result of the imposed mechanical deformation.

3.3.2. Cold Pressed and Sintered

We observed the same features discussed above, with respect to the hot-pressed urania, in the cold-pressed material. Two micrographs, Figures 15a and 15b, illustrate these points. Figure 15a is from $^{238}UO_2$ tested at 1400°C,

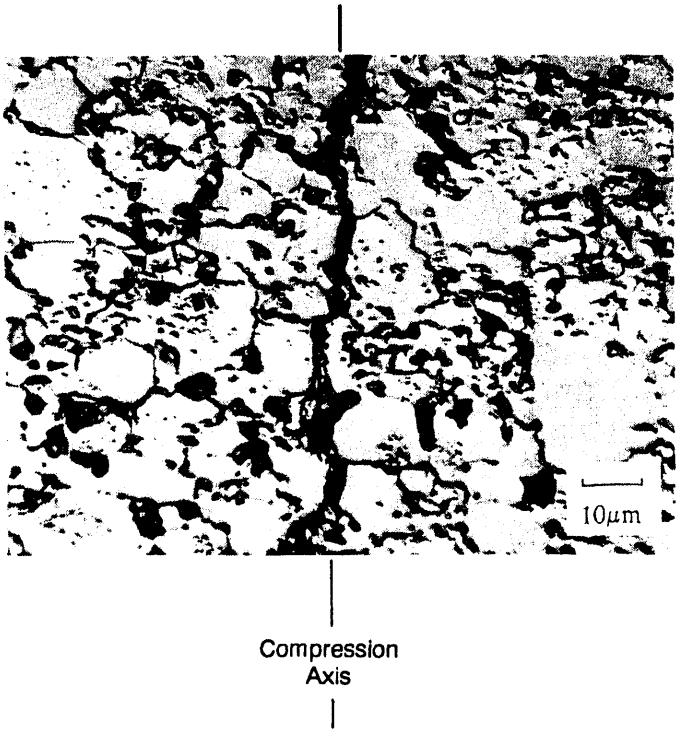

Figure 11a Photomicrograph showing intergranular cracking of a hot-pressed and grain-stabilized specimen deformed at 1400°C and a strain rate of $\varepsilon = 2.5 \times 10^{-4}\ s^{-1}$.

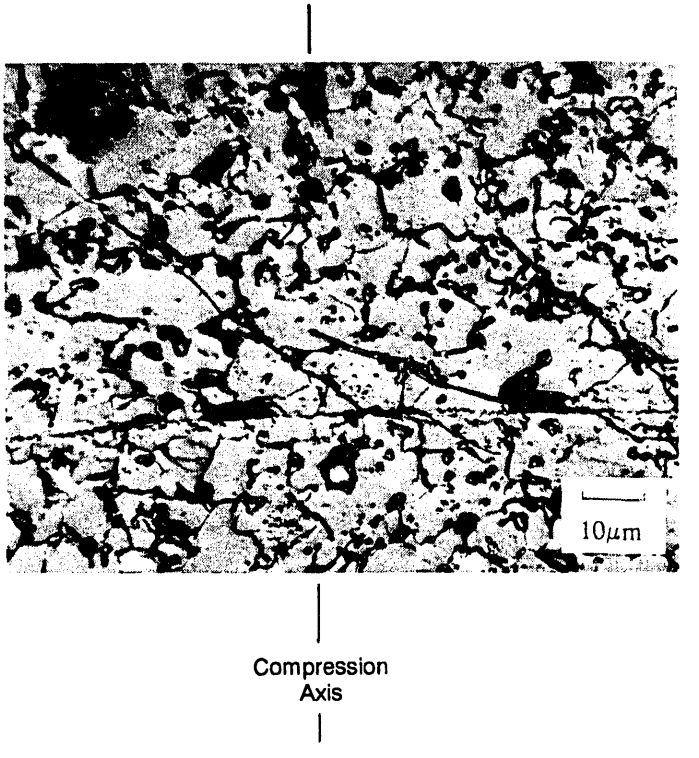

Figure 11b Photomicrograph showing transgranular cracking of a hot-pressed and grain-stabilized specimen deformed at 1400°C and a strain rate of $\varepsilon = 2.5 \times 10^{-4}\ s^{-1}$.

$\dot{\varepsilon}$=0.1 s^{-1}; Figure 15b shows urania deformed at 900°C and a strain rate of 2.5 x 10^{-4} s^{-1}. The fracture of the urania is intergranular at 1400°C, and again we observe a transgranular crack, likely from processing, normal to the compression axis. The fracture was largely transgranular at 900°C, and close examination of the micrograph shows that there are large displacements of parts of the same grain across the fracture surface, Figure 15b. This is in contrast to the transgranular cracks that we attribute to processing. In that situation the cracks did not open. Any displacements of one crack flank relative to the other were minimal.

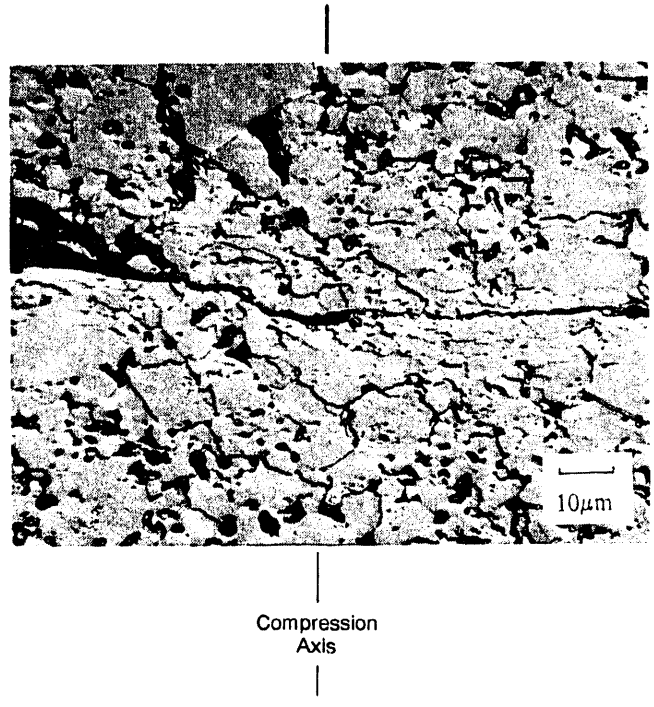

Figure 12 Evidence of recrystallization on the edges of a horizontal transgranular crack from a hot-pressed and grain-stabilized specimen deformed at 1400°C, ε = 2.5 x 10^{-4} s^{-1}.

Our observations, demonstrated by the different micrographs, indicate that there is no difference in the fracture behavior of the hot and cold pressed with respect to changes in temperature and strain rate. Thus, a single fracture map can be used to plot the behavior of these materials in temperature, strain-rate, and yield-stress space.

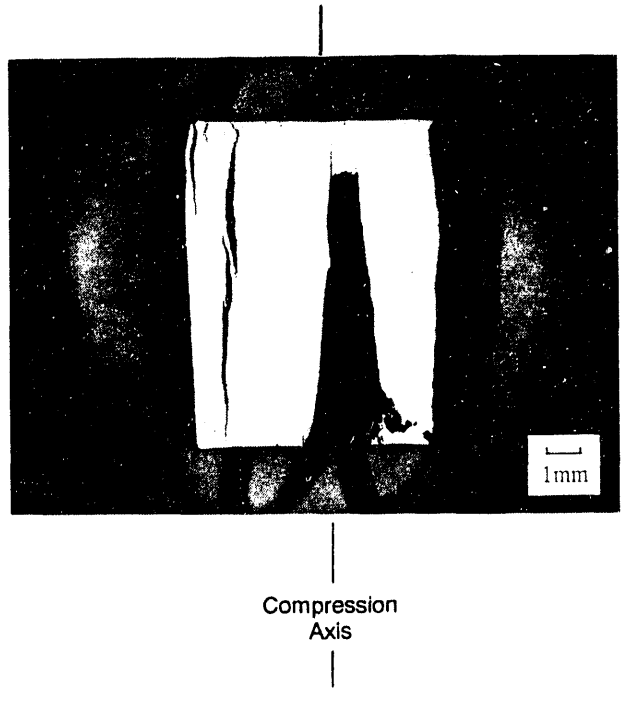

Figure 13 Low magnification micrograph taken from a cross section of a specimen deformed at 1000°C and a strain rate of ε = 2.5 x 10^{-4} s^{-1}.

4. Prediction of Yield Strength and Fracture Stress as a Function of Strain Rate and Temperature

4.1. Mechanical Threshold Stress Model

A model to predict the yield strength of materials as a function of strain rate and temperature has recently been proposed by

Compression Axis

Figure 14a Intergranular fracture in a specimen deformed at 1000°C and a strain rate of $\dot{\varepsilon} = 2.5 \times 10^{-4}\ s^{-1}$.

Compression Axis

Figure 14b Transgranular fracture in a specimen deformed at 1000°C and a strain rate of $\dot{\varepsilon} = 2.5 \times 10^{-4}\ s^{-1}$.

Follansbee and Kocks.[12] The model assumes that yielding occurs as a result of thermally activated dislocation motion. Thus, in principle this model should be appropriate for describing the temperature strain-rate dependencies of our $^{238}UO_2$. The model is referenced to the material's yield stress at 0 K and its mechanical threshold stress, which is independent of strain rate. The model describes how much thermal activation lowers the yield stress with respect to the mechanical threshold stress.

The Follansbee-Kock's mechanical threshold stress (MTS) model assumes that the yield stress of a material is comprised of the linear sum of two terms,

$$\frac{\sigma}{\mu} = \frac{\sigma_a}{\mu_0} + S(\dot{\varepsilon}, T)\frac{\hat{\sigma}}{\mu_0} \quad , \tag{1}$$

where

$$S = \left\{ 1 - \left[\frac{kT}{\mu b^3 g_0} \ln\left(\frac{\dot{\varepsilon}_0}{\dot{\varepsilon}} \right) \right]^{1/q} \right\}^{1/p} \quad . \tag{2}$$

The terms in these equations generally have their classic materials science meanings: μ is the shear modulus, b the Burger's vector, T temperature (K), k Boltzmans constant, and $\hat{\sigma}$ the mechanical threshold stress. There are several adjustable constants: p, q, and g_0 ; although the values of these constants are restricted by the principles of dislocation activity. Kocks, Argon, and Ashby[13] have shown that $0 \leq p \leq 1$ and $1 \leq q \leq 2$. Based on these arguments Follansbee[12] has set $p = 2/3$ and $q = 1$. We will use these values for p and q in our analysis of the urania.

Figure 16 is a schematic representation of the urania's stress/strain behavior. The two terms in (1) contribute to the yield stress of the urania, and then after yield, the urania flows perfectly plastically. In the complete version of the MTS model, finite material hardening is also modeled. However, because the urania's flow behavior is so close to elastic/perfectly plastic we have chosen not to consider any hardening behavior after yield. The first term results from athermal contributions to the urania's yield stress. This term is often called a friction or internal stress and results from dislocation interactions with grain boundaries, for example. The second term describes the effects of interactions between intrinsic dislocations and defects. These dislocation activities are thermally activated, and it is here that the temperature and strain-rate sensitivity of yield stress is accounted for. The parameter $\hat{\sigma}$, the mechanical threshold stress, represents the highest possible yield stress of the material. Thus, the term S

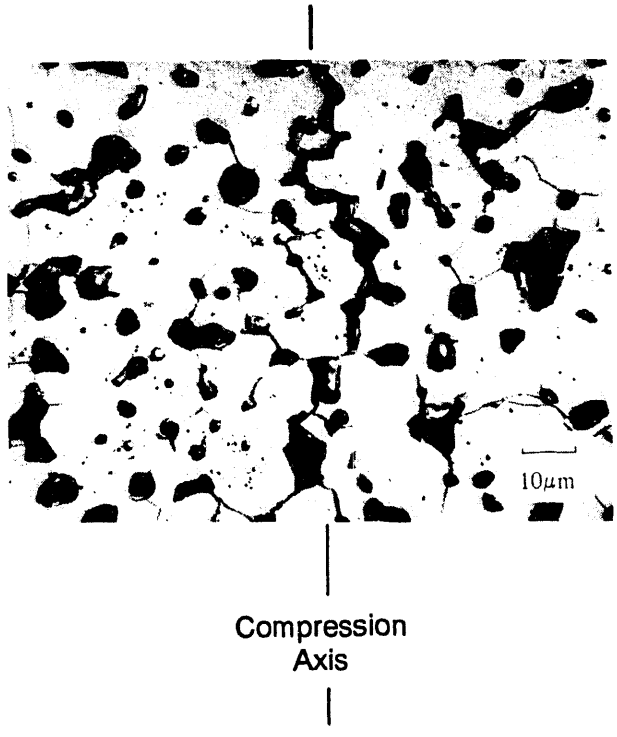

Figure 15a Intergranular fracture in a cold-pressed and sintered specimen deformed at 1400°C and a strain rate of $\dot{\varepsilon} = 0.1\ s^{-1}$.

Figure 15b Transgranular fracture in a cold-pressed and sintered specimen deformed at 900°C and a strain rate of $\dot{\varepsilon} = 2.5 \times 10^{-4}\ s^{-1}$.

will always be less than one and have its smallest values for lower strain rates and higher temperatures.

4.2. MTS Analysis of the Radford and Terwilliger Data

The most extensive measurement of yield stress data for $^{238}UO_2$, as a function of strain rate and temperature, has been by Radford and Terwilliger[6] (R&T). They examined four different strain rates and temperatures between 600° and 1600°C. These data are ideally suited for determining the coefficients necessary for evaluation of the MTS model. However, the R&T data were taken for a material that we estimate to be 97% dense and that had a grain size of 17 μm. In addition, our material had a stoichiometry that was slightly different than 2.0. Our approach was to first modify the entire collection of R&T's data, properly accounting for the grain size, porosity, and stoichiometry appropriate to our urania material, and then fit the MTS model to the corrected data set.

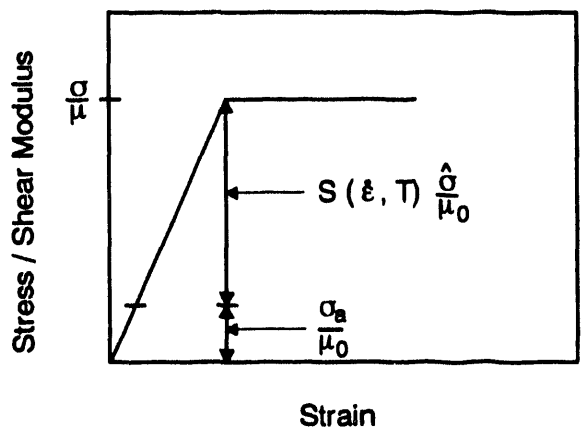

Figure 16 A schematic representation of the components contributing to the yield stress in the MTS model.

4.2.1. Grain Size

Yield stress data generated by R&T were taken from material of three different grain sizes: 17, 9, and 6.3 μm and seven temperatures: 800°, 900°, 1000°, 1100°, 1200°, 1300°, and 1400°C. This is shown in Figure 17. These data are plotted versus $1/\sqrt{d}$ where d is the grain size of the material. As one can see, the data are well described by a series of parallel straight lines, each line fitting the data for a particular temperature and are thus described by the equation:

$$\sigma = \alpha + \beta/\sqrt{d} \quad , \qquad (3)$$

where σ is the yield strength, d is the grain size, and α and ß are constants. Because the lines are parallel, ß is constant with respect to temperature, and the variation of yield strength with temperature in these data is described by the term α. We found that ß = 391 MPa√μm.

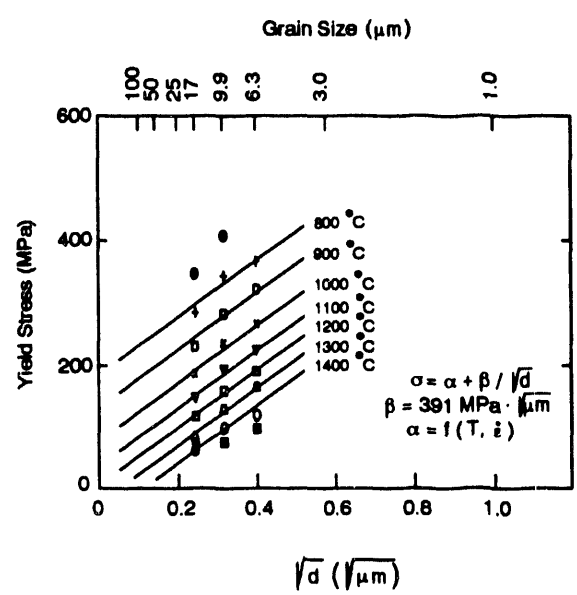

Figure 17 Yield stress data of R&T for different grain size materials.

Because ß is constant with respect to temperature, the effect of grain size is accounted for by a scalar sum to the measured yield stress, for a given grain size. The sum is the same for all temperatures. The values of α corresponding to ß = 391 MPa$\sqrt{\mu m}$ are negative for temperatures of 1300° and 1400°C. Physically, this is unrealistic and it indicates that this law is not applicable for all grain sizes. The grain size averaged between our two materials was 6.15 μm, $1/\sqrt{d}$ = 0.403. This is slightly outside the specific range of R&T's experiments; however, we believe that (3) is still valid. Solving (3), noting that the grain sizes of R&T's and our material were 17 and 6.15 μm, respectively, we found that increasing all yield strengths by 62.76 MPa would account for grain size differences between the R&T and Los Alamos materials.

4.2.2. Porosity Effects

R&T do not specify the porosity of their specimens. We estimate that they were working with material that was approximately 97% of theoretical density, while our material has an average theoretical density of 85%. We have based our porosity correction on two factors: the physical porosity and the stress concentration that results from porosity present in the material. We believe that the latter effect is particularly important because our material is 15% porous, which is a high degree of porosity. If the material was of high density, ~ 97% dense or 3% porosity, the stress concentration would only affect a small volume fraction of material. Thus, the overall yield stress should be only mildly influenced. With the high degree of porosity of this material, the stress concentration will affect a large fraction of urania. Thus, the stress concentration should noticeably lower the yield stress.

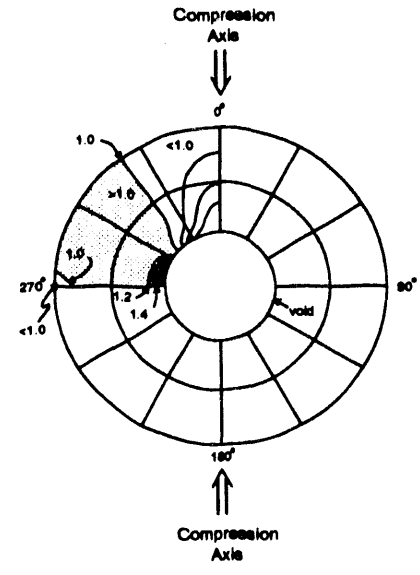

Figure 18 Stress concentration contours resulting from a spherical void in a homogeneous elastic $^{238}UO_2$ body.

For a spherical void in a material, the volume fraction and the area fraction of porosity are equivalent. Thus, we have decreased the yield stress of the R&T data by 12%. This is the difference in porosity between the two materials.

Because the porosity in our material is 'compact' or nearly spherical, we believe that it is appropriate to model it as a spherical void in a homogeneous medium. In three dimensions, assuming isotropic elasticity, this situation results in a stress concentration of 2.05. We have also calculated this stress concentration using the exact elastic constants of the $^{238}UO_2$. The stress contours predicted by the calculation are shown in Figure 18. Because of symmetry we have plotted the contours only over one quarter of the space. One should note that the contours have been normalized to the far-field applied stress. Thus, contours of value greater than one (1)

indicate a stress concentration. There is a large region for which this is the case, shown by the light shading. In a smaller region the stress concentration is highest between 1.2 and 1.4, shown with the heavier shading. We have had to use personal judgment to quantify the strength of this concentration with respect to measured yield strength of the urania. We believe that it is appropriate to decrease the yield strength by 20% as a result of the concentration. Combining the effects of that result from porosity thus necessitates correcting the R&T data downward by 32%.

4.2.3. Stoichiometry

Both Nadeau[3] and Byron[7] have measured the strength of polycrystalline $^{238}UO_2$ as a function of stoichiometry and temperature. Byron's experiments were for the specific composition $^{238}UO_{2.02}$, while Nadeau examined a range of compositions from $^{238}UO_{2.00}$ to $^{238}UO_{2.2}$. The strength of urania drops rapidly as the urania becomes hyperstoichiometric. For example, Nadeau found that if the composition was between $^{238}UO_{2.012}$ and $^{238}UO_{2.057}$, the strength was decreased on an average by ~30%. Byron's results were consistent. He found that the strength of $^{238}UO_{2.02}$ was also on average almost 30% less than that for the stoichiometric material. From the stoichiometric analysis of our specimens, the compression experiments began with $^{238}UO_{2.010\text{-}1.991}$. During the experiment the specimens were reduced through exact stoichiometry to ~ $^{238}UO_{1.995}$. The specific stoichiometry is thus unknown for any specific stage of the deformation process. However, it was always very close to exactly stoichiometric, within the apparent scatter of the measurement and the initial oxygen stoichiometry. The greatest deviation was measured as $^{238}UO_{1.989}$ for a cold-pressed and sintered specimen tested at 1400°C and $\dot{\varepsilon} = 2.5 \times 10^{-4}\ s^{-1}$. This deviation from exact stoichiometry was only slightly greater than the variation we observed in material starting composition, and the deviation did not appear to have any effect on our measured stress/strain response. Thus, these data were not given any correction for stoichiometry.

4.2.4. Corrected Data

Correcting the data of R&T by the factors properly describing grain size, porosity, and stoichiometry brings it into close agreement with our current results. Their results are plotted with our data in Figure 19. Not only are the absolute stress levels in accord, but so are the curvatures describing shapes for the change in yield stress as a function of temperature for a given strain rate. We will use the R&T data, as it is presented in Figure 19, for the evaluation of the MTS model for yield strength.

4.3. MTS Model Coefficients

Many of the constants appearing in (1) and (2) are known physical constants and have been previously evaluated. We can also estimate or make assumptions concerning the other terms. For example, we have assumed that σ_a is equal to 30 MPa. If one were to extend the yield stress/temperature data to high temperatures and low strain rates, it would asymptotically approach this value. The value of $\dot{\varepsilon}_0$ can also be assumed. This parameter represents an arbitrarily high

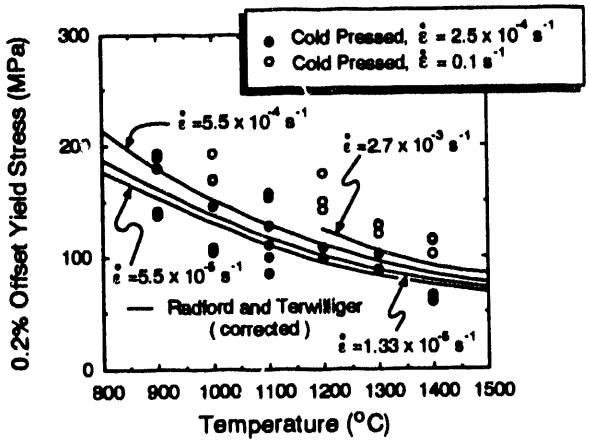

Figure 19 Yield stress data of R&T corrected for grain size, porosity, and stoichiometry plotted with the Los Alamos cold-pressed and sintered data.

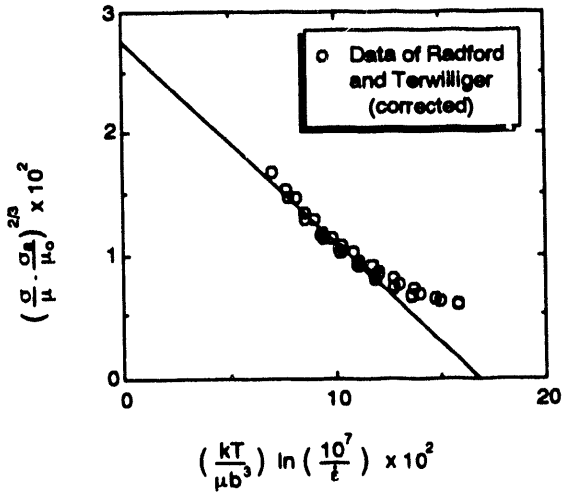

Figure 20 A plot of (4) with the linear fit that determined $(\sigma/\mu_0)^{2/3}$ and $1/g_0$ for the MTS model.

strain rate, within physical reason. In his work with copper, Follansbee selected $\dot{\varepsilon}_0 = 10^7$ s^{-1}. We will use the same value. Finally, μ_0 is the shear modulus of the urania at 0 K. Typically the material moduli increase linearly with decreasing temperature. As the temperature approaches 0 K, however, the moduli cease to increase and remain constant. Thus, μ_0 has been assigned the value of the shear modulus at 100 K. We can now rearrange (1) in the following form, substituting p = 2/3 and q = 1:

$$\left(\frac{\sigma}{\mu} - \frac{\sigma_a}{\mu_0}\right)^{2/3} = \left(\frac{\hat{\sigma}}{\mu_0}\right)^{2/3} - \frac{1}{g_0}\left(\frac{\hat{\sigma}}{\mu_0}\right)^{2/3}\left[\frac{kT}{\mu b^3}\ln\left(\frac{\dot{\varepsilon}_0}{\dot{\varepsilon}}\right)\right] \quad . \tag{4}$$

From the data of R&T, we know the yield stress, σ, for particular strain rates and temperatures. Thus, the only parameters that cannot be evaluated from literature data or for which we have not assumed values are $\hat{\sigma}$ and $1/g_0$. If we collectively plot individual yield datum for specific temperatures and strain rates as $(\sigma/\mu - \sigma_a/\mu_0)^{2/3}$ versus $kT/\mu b^3 \ln(\dot{\varepsilon}_0/\dot{\varepsilon})$, as in Figure 20, (4) becomes the equation for a linear fit to the data. The intercept of the fit at 0 has the value $(\hat{\sigma}/\mu_0)^{2/3}$ and the slope of the fit is $1/g_0(\hat{\sigma}/\mu_0)^{2/3}$. Thus, from the linear fit we can complete our evaluation of the constants needed for using the MTS model to predict yield strength as a function of temperature and strain rate. As one can see in Figure 20, all of the data cannot be fit to a line. We have opted to match our data at higher strain rates and lower temperatures. The deviation from linear behavior is not atypical and has been observed in all materials Follansbee has studied at high temperatures and low strain rates. A summary of values of all of the

coefficients, including those obtained from the fit as described and illustrated above, is given in Table II.

Table II
Coefficients for Use in the MTS Model

Coefficient	MTS value	Source
σ_a	30 MPa	Ref. 6
$\hat{\sigma}$	441.36 MPa	linear fit to (4)
$\mu(T)$	$\mu = 9.39\times10^4 \left(1+\frac{T-300}{3080}(-.35)\right)$ MPa	Ref. 1
μ_0	9.60 x 10^4 MPa	assumption and Ref. 1
$1/g_0$	5.5 5	linear fit to (4)
k/b^3	0.2381 MPa/°K	Ref. 1
$\dot{\varepsilon}_0$	10^7	assumption and Ref. 12
p	2/3	Refs. 12 and 13
q	1	Refs. 12 and 13

4.4. Predictions of the MTS Model

We have calculated the values of yield stress, predicted by the MTS model (2) (3) and the coefficients listed in Table II, for the different strain rates used by R&T over the temperature range 800° to 1600°C. These results are superimposed over the corrected data of R&T in Figure 21. The results of the MTS model are really quite satisfactory considering that we are using a relatively simple analytic function to model $\sigma(\dot{\varepsilon}, T)$. The absolute yield stress levels are predicted well; however, there is a greater curvature to the experimental data than shown by the model. The greatest errors in prediction occur at the lowest strain rates, $\dot{\varepsilon}$ = 1.3333 x 10^{-5}, 5.5 x 10^{-5}, and 5.5 x 10^{-4} s^{-1}, above 1300°C. This was to be expected from the range of data that we selected on which to perform the linear fit.

4.5. Urania $^{238}UO_2$, Deformation/Fracture/Yield Strength Maps

The bend bar fracture data of Evans and Davidge[8] and Canon *et al.*[9] indicate that tensile fracture occurs at about 145 MPa for 97% dense urania. This fracture strength appeared to be insensitive to strain rate and only slightly sensitive to temperature. There was a very slight increase in the fracture strength of about 10 MPa from 800° to 1500°C in the data of Canon *et al.*[9] Above

1500°C there was a very rapid decrease in the fracture strength, down to 40 MPa at 1800°C. The exact temperature at which the strength decrease begins appears to be a function of strain rate. The lower the strain rate the lower the temperature. The bend bars from which these data were obtained behaved in a purely elastic fashion up to about 1200°C and then began to show very small amounts of plastic deformation. Even at 1500° to 1600°C, the bars deformed plastically by only 1% strain before fracturing. The rapid strength decrease above 1500°C and the tensile plastic deformation appear to be associated with grain boundary sliding and grain boundary fracture mechanisms. Metallographic observations of Canon *et al.*[9] and by ourselves are consistent with the mechanical strength measurements; at and above 1400°C extensive intergranular fracture is seen. This behavior is promoted by the lower strain rates.

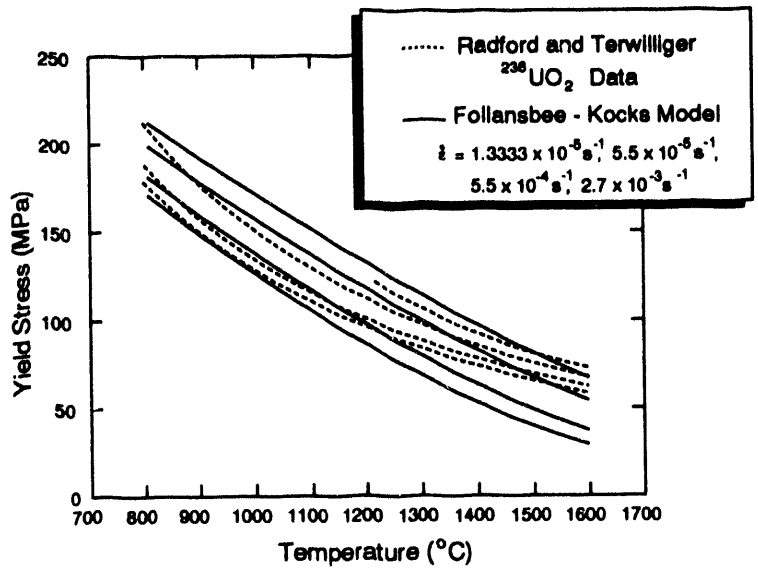

Figure 21 A comparison of the R&T data with the predictions of the MTS model.

Roberts and Ueda[10] examined the effects of porosity on fracture strength by using naphthalene to enforce the porosity and then burning it away during the sintering process. The fracture strengths of their bend bars were much less than those reported in References 8 and 9. All of the data are at equivalent high densities, ~97% dense. Roberts and Ueda's fracture strength of 145 MPa for lower density material, ~87% dense, matches that for 97% theoretical density material from References 8 and 9. We believe that the material used by Roberts and Ueda had a closed cell porosity. Thus, the process of burning out the naphthalene likely damaged the urania. At lower density the porosity is much more open and little damage occurs. That is why the strengths are higher and approach those of the other researchers for high density material. It thus appears that the tensile fracture strengths and deformation and fracture mechanisms are largely independent of porosity. Accordingly, we will use these data[8,9] to construct our plastic deformation/ fracture/yield strength map.

Macroscopically, material stressed in pure compression is not subject to tensile loads. Thus, even brittle materials can, in compression, bear large loads. That is why we could measure compressive yield strengths in excess of 200 MPa and see large plastic deformations in material that yielded below 200 MPa, for the Los Alamos $^{238}UO_2$. As the urania is compressed, its length decreases and accordingly, the diameter needs to increase. One must maintain compatibility between grains to accomplish this process, which can only be done if the material is able to deform. Local heterogeneous tensile stresses arise on the length-scale of grains, if the extent of

deformation from dislocation activity is inadequate. This tensile stress will initiate fracture in the compression, as we observed when the yield stress exceeded 200 MPa. In this case the fracture is always parallel to the axis of compression. Byron[7] extended the temperature range of his compression experiments on stoichiometric urania to 2000°C to determine at what temperature grain boundary sliding, followed by loss of compatibility and hence fracture, by grain boundary decohesion occurred. In this case, the deformation is accomplished by diffusion processes rather than dislocation activity. A rapid decrease in strength is observed in Byron's data above 1800°C, and he associates it with such a mechanism.

The plastic deformation/fracture/yield strength maps were constructed from the above fracture observations and the MTS model. First, we have predicted the yield strength of the $^{238}UO_2$ for strain rates of $\dot{\varepsilon} = 10^{-5}$, 10^{-3}, 10^{-1}, 10, and 10^{3} s^{-1} and temperatures between 800° and 1600°C using the MTS model. The curves in Figures 22a and 22b are the yield stresses predicted by the MTS model for different strain rates as a function of temperature. As we saw in Figure 21, these should be accurate predictions for strain rates above 10^{-2} s^{-1} at all temperatures. We know that the fracture behavior of the urania is dependent on whether the stress state is tensile or compressive; accordingly, we have constructed separate maps Figure 22a for compression and Figure 22b for tension.

In compression, we observed fracture when the yield stress was above 200 MPa. This stress level did not appear to be dependent on temperature or strain rate, hence, the boundary between yield followed by plastic deformation and fracture is a horizontal line in this space. Grain boundary sliding and separation events were not observed until 1800°C in compression; thus, there is only one region of fracture on this map. Although there is only one fracture region in compression, the path that the fracture takes does change as a function of temperature. Below 1100°C the fracture takes a generally transgranular path. On the other hand, we observed intergranular fracture at 1300° and 1400°C. These observations are indicated schematically in Figure 22a.

In tension, fracture was observed between 140 MPa and 150 MPa, the fracture stress higher at higher temperature. The behavior was again strain-rate insensitive. At temperatures above 1400°C, the tensile behavior of the urania was not as well defined. In this region, grain boundary sliding becomes a dominant mechanism, and the stress at which fracture occurs rapidly decreases with a slight increase in temperature. The grain boundary sliding and decohesion mechanisms are strain-rate sensitive, and we have drawn individual curves for the different strain rates reported by Canon *et al.*[9] There is no evidence of large amounts > 2% strain of plastic deformation in tension. Thus, although yield has taken place, one could approximate the material behavior as elastic up to fracture for all temperatures. The data of Canon *et al.*[9] at high temperatures, where there is a rapid strength decrease resulting from grain boundary decohesion, do not appear to be consistent with our predictions of yield strength based on the MTS model. Our predicted yield strengths appear to be too low. However, one must remember that this is a temperature/strain rate regime where we observed the largest deviation between the model and experimental data. That is why these strength predictions are shown as dotted lines. The yield stresses predicted by the model were in fact too low. Our experimental yield stresses in

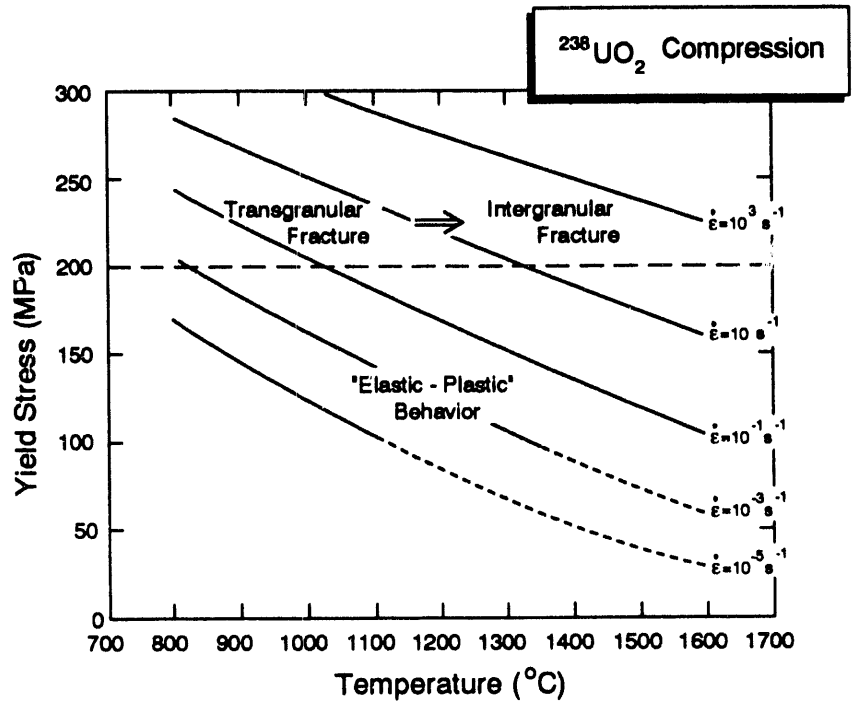

Figure 22a An engineering map, for compressive stress states, illustrating regions of different $^{238}UO_2$ fracture behavior superimposed with MTS-model predictions of $^{238}UO_2$ yield strength.

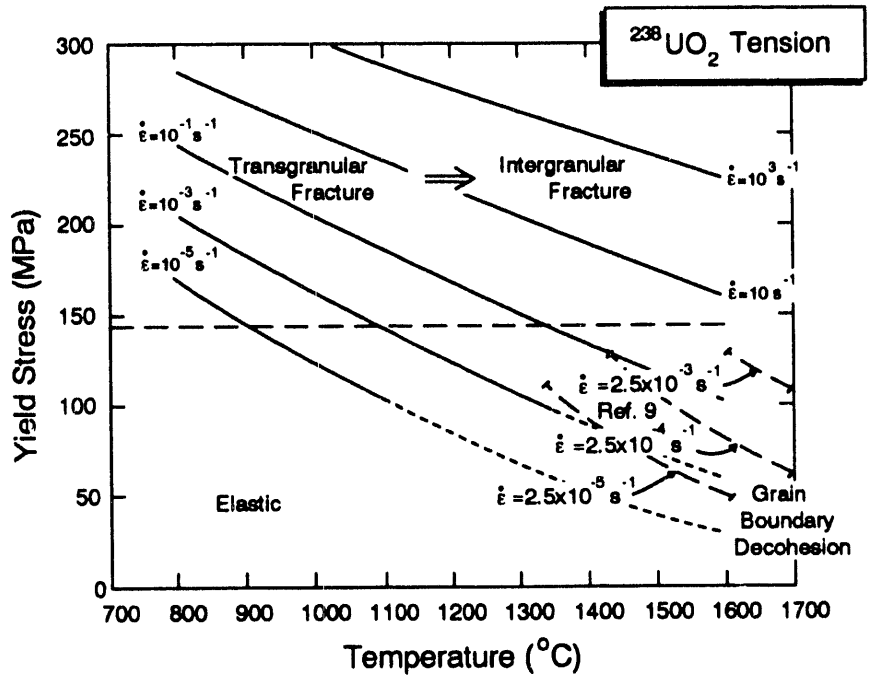

Figure 22b An engineering map, for tensile stress states, illustrating regions of different $^{238}UO_2$ fracture behavior superimposed with MTS-model predictions of $^{238}UO_2$ yield strength.

compression, for $\dot{\varepsilon}$ = 2.5 x 10^{-4} s^{-1} at 1300° and 1400°C, were approximately 100 MPa and 70 MPa, respectively (cold-pressed material). These yield strengths are consistent with the strength levels reported by Canon *et al.*[9] Thus, we believe that the tensile fracture map (Figure 22b), constructed largely from literature fracture observations, is accurate for the Los Alamos-fabricated $^{238}UO_2$. These maps are applicable for either the cold- or hot-pressing fabrication conditions.

5. Comparison of $^{238}UO_2$ with $^{238}PuO_2$ and $^{239}PuO_2$

5.1. Behavior of Plutonia and Urania

Petrovic *et al.*[14] have performed an extensive series of compression experiments on $^{238}PuO_2$. The specimens were tested at, or very close to, a strain rate of 10^{-3} s^{-1}. They reported very limited ductility in these specimens, strains between 0.0018 and 0.0061, after the proportional limit was reached. Thus, they reported ultimate stresses rather than yield stresses for their experiments. Experiments were done at temperatures of 1000°, 1200°, 1300°, 1400°, and 1500°C. These results are shown with the ultimate stresses that we measured for the $^{238}UO_2$ in Figures 23a and 23b, hot pressed and grain stabilized and cold pressed and sintered, respectively. We have plotted both our yield and ultimate strength data for the urania in these figures. At 1000°C the ultimate strengths of all three materials match very closely, while the urania yield strength is slightly below the ultimate strength of the plutonia. For temperatures above 1200°C, the ultimate strength of the plutonia falls below that of the urania, until at 1400°C the ultimate strength of the urania is about twice that of the plutonia.

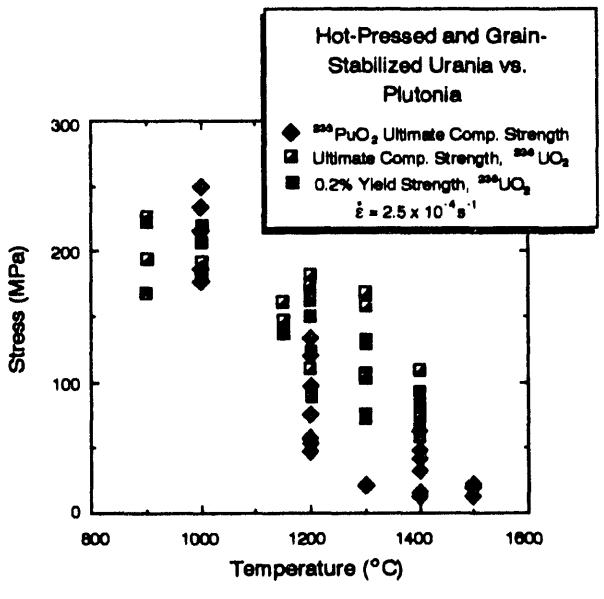

Figure 23a The ultimate compressive strength of $^{238}PuO_2$, Petrovic *et al.*, compared to the strength of hot-pressed and grain-stabilized $^{238}UO_2$, this study.

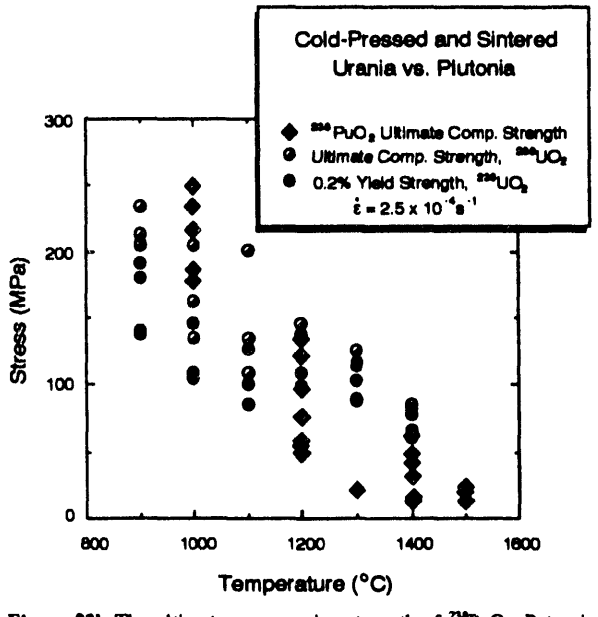

Figure 23b The ultimate compressive strength of $^{238}PuO_2$, Petrovic *et al.*, compared to the strength of cold-pressed and sintered $^{238}UO_2$, this study.

Petrovic and Land[15] have performed additional experiments using $^{239}PuO_2$ that shed light on the mechanism responsible for the decay of the strength of the plutonia relative to the urania. Specifically, they tested $^{239}PuO_2$ at different strain rates and then calculated the strain-rate sensitivity exponent. At 1200°C the value of m was 37, indicative of thermally activated dislocation activity. But at 1400°C they found m = 1.82, which is characteristic of grain boundary sliding. This is strong evidence that grain boundary decohesion is likely responsible for the rapid strength decrease of the plutonia above 1200°C. We know from literature data that this does not occur in the $^{238}UO_2$ until one reaches at least 1800°C. Petrovic and Land conducted diametral compression tests on $^{239}PuO_2$ cylinders as well. Diametral compression, as opposed to the standard direct compression, results in tensile stresses across the loading axis in the specimen interior. From such experiments Petrovic and Land report an ultimate tensile strength of 28 MPa at 800°C, decreasing approximately linearly to 16 MPa at 1400°C. These strengths are much lower then the bend-bar tensile strengths reported for the $^{238}UO_2$.[8,9]

We believe on this basis that $^{238}UO_2$ is an excellent mock material for $^{238}PuO_2$ in compression below 1200°C. Not only are the ultimate strengths identical but the yield behaviors are consistent as well. Above 1200°C the strength of the urania is greater than that of the plutonia, although the match is still very close. We think that performances under impact conditions should be comparable. If these two ceramics are subject to tensile loading, the agreement between materials will be quite poor. The urania is simply too strong with a tensile strength about seven (7) times that of the plutonia. The extreme weakness of the plutonia is again indicative of exceptionally weak grain boundaries.

5.2. Fracture Map of Plutonia

We have constructed deformation/fracture maps for $^{238}PuO_2$ in compression (Figure 24a) and $^{239}PuO_2$ in tension (Figure 24b) based on the yield data of urania and the reported plutonia fracture behavior.[14,15] There is insufficient strain-rate sensitivity data on the plutonia to be able to determine the coefficients necessary for evaluation of the MTS model. We believe that the yield stress/strain-rate/temperature curves that we have constructed for the $^{238}UO_2$ should closely model the behavior of the plutonia. This is based on the almost exact agreement of the mechanical properties of these two materials at 1000°C, before grain boundary mechanisms dominate the behavior of the $^{238}PuO_2$. Thus, the MTS yield strength predictions for the $^{238}UO_2$ provide the basis of the plutonia deformation/fracture map. If grain boundary decohesion does not occur, the plutonia appears to fracture in compression from heterogeneous compatibility-induced tensile stresses at 200 MPa. This condition is indicated by the horizontal line in Figure 24a.

Petrovic *et al.*[14] also observed a transition between transgranular and intergranular fracture near 1000°C. This is indicated schematically in Figure 24a. Intergranular fracture intercedes quickly for the plutonia with increasing temperature. The border for the occurrence of this mechanism is indicated by a dashed line for a strain rate of $\dot{\varepsilon} = 10^{-3}\ s^{-1}$. This border is drawn from the experimental data of Petrovic *et al.*[14] and will be very sensitive to strain rate. From the extent of the strain-rate sensitivity shown by the urania, when a grain boundary decohesion mechanism

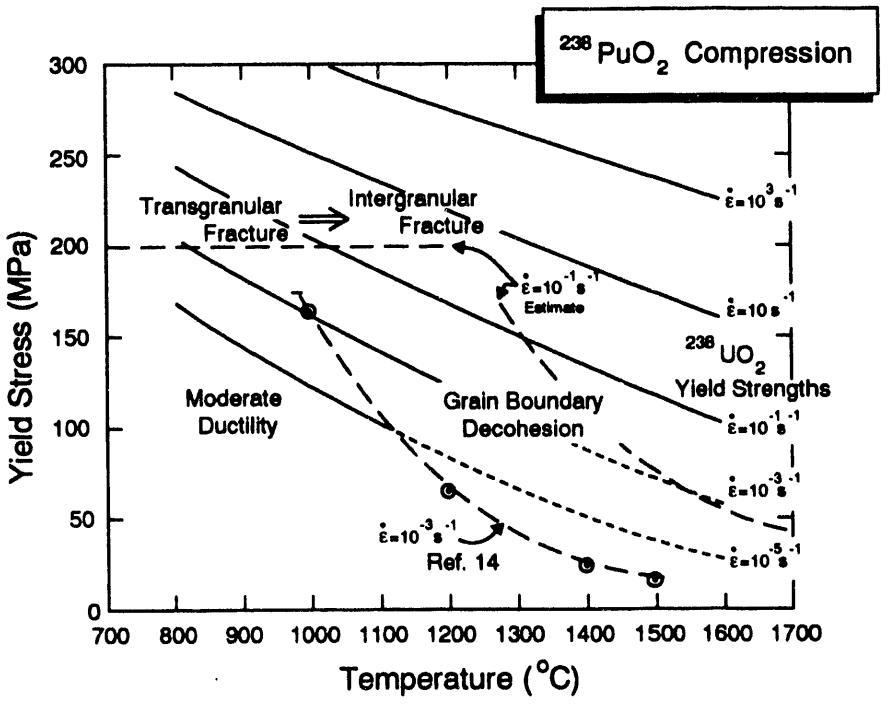

Figure 24a An engineering map, for compressive stress states, illustrating regions of different $^{238}PuO_2$ fracture behavior superimposed with MTS-model predictions of $^{238}UO_2$ yield strength.

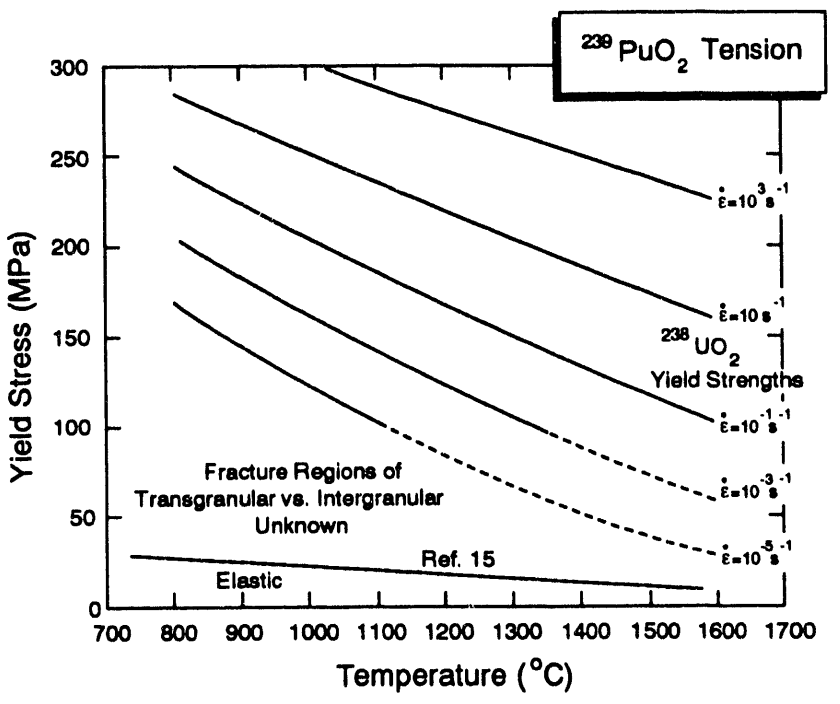

Figure 24b An engineering map, for tensile stress states, illustrating regions of different $^{239}PuO_2$ fracture behavior superimposed with MTS-model predictions of $^{238}UO_2$ yield strength.

dominates fracture, we have estimated where this border would lie for a strain rate of 0.1 s^{-1}. The effect is a horizontal shift of the boundary upwards in temperature by 300°C. Figure 24b is the tensile map constructed from the $^{239}PuO_2$ data. It is very simple. Fracture occurs once a 30-MPa tensile stress has been reached for all temperatures.

6. Conclusions

1. Our compression experiments have demonstrated that either of the Los Alamos processing schedules, hot pressed and grain stabilized or cold pressed and sintered, produce equivalent material. The yield and ultimate strengths that we measured for these two materials as a function of strain rate and temperature were equivalent. In addition our metallographic observations showed that the two materials had the same structure. Their grain sizes were equivalent and the distribution and morphology of porosity were identical. Finally, our observations of crack path comparing the two materials were consistent. Both materials fractured along a transgranular path when the test temperatures were < 1100°C. The fracture paths then transitioned to a largely intergranular nature for T > 1200°C.

2. Urania will be an excellent mock material for $^{238}PuO_2$ if the loading stress states are compressive. These materials have identical yield and ultimate strengths below ~ 1200°C when deformed at a strain rate of 10^{-3} s^{-1}. At this strain rate the plutonia loses strength relative to the urania for T > 1200°C. This loss of strength is a result of grain boundary decohesion mechanisms and is hence dependent on strain rate. We have estimated that at impact strain rates, the strength decrease should not occur below a temperature of 1400°C. Thus, in experimental impact engineering safety studies, the performance of $^{238}UO_2$ can be expected to be equivalent to $^{238}PuO_2$.

3. We believe, based on the MTS model predictions of yield stress as a function of strain rate and temperature, that the urania will not deform plastically during any impact tests. The MTS model predicts $^{238}UO_2$ yield strengths higher than 200 MPa whenever $\dot{\varepsilon} > 100$ s^{-1} for temperatures up to 1600°C. It would be most unusual if the impact strain rates were ever below 10^3 s^{-1}. We always observed brittle fracture in our compression experiments when the yield stress was above 200 MPa.

4. In a loading condition that produces a tensile stress state, the $^{238}UO_2$ will not be an appropriate simulant for the $^{238}PuO_2$. A comparison of the literature data for these materials indicates that $^{239}PuO_2$ fractures at about 20% of the tensile strength of urania. The $^{238}PuO_2$ contains thermal cracking which is nonexistent in the $^{239}PuO_2$; hence, the tensile strength of $^{239}PuO_2$ is a best case scenario. Thus, a urania simulant would be far too strong to accurately mock the plutonia under tension.

5. Our measurements showed the Los Alamos urania to have a stoichiometry of almost exactly $^{238}UO_2$. Our experimental strength results are therefore fully consistent with the literature data. If this stoichiometry is maintained during engineering component experiments, with an inert argon atmosphere for example, the deformation/fracture maps will remain valid. In addition, the yield strengths will remain at the levels that are cited in this report.

References

1. H. J. Frost and M. F. Ashby, "Oxides with the Fluorite Structure: UO_2 and ThO_2," *Deformation-Mechanism Maps*, Pergamon Press, New York, NY, pp. 93-97, 1982.

2. A. H. Heuer, R. J. Keller, and T. E. Mitchell, "On the Slip Systems in Uranium Dioxide," in *Deformation Processes of Minerals, Ceramics and Rocks*, D. J. Barber and P. G. Meredith, eds. Unwin Hyman, pp. 377-390, 1990.

3. J. S. Nadeau, "Dependence of Flow Stress on Nonstoichiometry in Oxygen-Rich Uranium Dioxide at High Temperatures," *J. Amer. Ceram. Soc.* **52**, pp. 1-7 (1969).

4. J. F. Byron, "The Yield and Flow of Single Crystals of Uranium Dioxide," *J. Nuclear Matls.* **28**, pp. 110-114 (1968).

5. R. J. Keller, T. E. Mitchell, and A. H. Heuer, "Plastic Deformation in Nonstoichiometric UO_{2+x} Single Crystals - II. Deformation at High Temperatures," *Acta Metall.* **36**, pp. 1073-1083 (1988).

6. K. C. Radford and G. R. Terwilliger, "Compressive Deformation of Polycrystalline UO_2," *J. Amer. Ceram. Soc.* **58**, pp. 274-278 (1975).

7. J. F. Byron, "Yield and Flow of Polycrystalline Uranium Dioxide," *J. Nuclear Matls.* **27**, pp. 48-53 (1968).

8. A. G. Evans and R. W. Davidge, "The Strength and Fracture of Stoichiometric Polycrystalline UO_2," *J. Nuclear Matls.* **33**, pp. 249-260 (1969).

9. R. F. Canon, J. T. A. Roberts, and R. J. Beals, "Deformation of UO_2 at High Temperatures," *J. Amer. Ceram. Soc.* **54**, pp. 105-112 (1971).

10. J. T. A. Roberts and Y. Ueda, "Influence of Porosity on the Deformation and Fracture of UO_2," *J. Amer. Ceram. Soc.* **55**, pp. 117-124 (1972).

11. J. T. A. Roberts, "Brittle Fracture of Oxide Nuclear Fuel," *J. Nuclear Matls.* **47**, pp. 125-128 (1973).

12. P. S. Follansbee and U. F. Kocks, "A Constitutive Description of the Deformation of Copper Based on the Use of the Mechanical Threshold Stress as an Internal State Variable," *Acta Metall.* **36**, pp. 81-93 (1988).

13. U. F. Kocks, A. S. Argon, and M. F. Ashby, "Thermodynamics and Kinetics of Slip," *Prog. Mater. Sci.* **19**, Pergamon Press, NY (1975).

14. J. J. Petrovic, S. S. Hecker, C. C. Land, and D. L. Rohr, "Mechanical Properties of $^{238}PuO_2$," Los Alamos National Laboratory Report LA-6529 (April 1977).

15. J. J. Petrovic and C. C. Land, "High Temperature Deformation of Stoichiometric $^{239}PuO_2$," *J. Amer. Ceram. Soc.* **63**, pp. 201-208 (1980).

Doc I

DATE FILMED

8/18/94

END